Flat Plate Thermal Solar Collector Efficiency: Transient Behavior Under Working Conditions. Part I: Model Description And Experimental Validation

M.C Rodríguez-Hidalgo, P.A. Rodríguez-Aumente, A Lecuona, G.L. Gutiérrez-Urueta, R Ventas

Accepted Manuscript

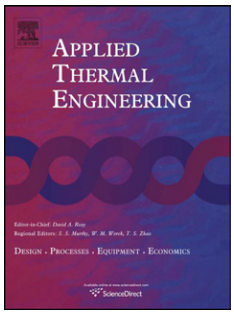

Title: Flat Plate Thermal Solar Collector Efficiency: Transient Behavior Under Working Conditions. Part I: Model Description And Experimental Validation

Authors: M.C Rodríguez-Hidalgo, P.A. Rodríguez-Aumente, A Lecuona, G.L. Gutiérrez-Urueta, R Ventas

PII: S1359-4311(11)00191-8

DOI: 10.1016/j.applthermaleng.2011.04.003

Reference: ATE 3498

To appear in: *Applied Thermal Engineering#*

Received Date: 30 October 2010

Revised Date: 12 February 2011

Accepted Date: 6 April 2011

Please cite this article as: M.C Rodríguez-Hidalgo, P.A. Rodríguez-Aumente, A Lecuona, G.L. Gutiérrez-Urueta, R. Flat Plate Thermal Solar Collector Efficiency: Transient Behavior Under Working Conditions. Part I: Model Description And Experimental Validation, Applied Thermal Engineering (2011), doi: 10.1016/j.applthermaleng.2011.04.003

FLAT PLATE THERMAL SOLAR COLLECTOR EFFICIENCY: TRANSIENT BEHAVIOR UNDER WORKING CONDITIONS.

PART I: MODEL DESCRIPTION AND EXPERIMENTAL VALIDATION

Rodríguez-Hidalgo, M. C., Rodríguez-Aumente, P. A. [*], Lecuona, A., Gutiérrez-Urueta, G. L., Ventas, R.

Universidad Carlos III de Madrid. Departamento de Ingeniería Térmica y de Fluidos. Grupo ITEA

Avda. Universidad 30, 28911 Leganés, Madrid, Spain

ABSTRACT

The efficiency of a solar collector is a key factor for the performance of thermal facilities. As the weather conditions vary continuously during the day, the instant collector efficiency depends not only on the components employed in its construction but also on the actual environmental conditions, the hot water temperature and aging. An experimental research was performed to describe the transient behavior of a flat plate collector field under outdoor working conditions.

A transient collector model was assembled using thermal resistances and capacitances. Three thermocouples were added to measure the centre point temperature of the glass cover, box back surface and absorber plate of one of the

[*] Corresponding author: Phone: +34 91 624 9406 Fax: +34 91 624 9430 E-mail: aument@ing.uc3m.es

collectors. Using this information, the parameters of a detailed thermal network model were determined.

The model useful heat and thermal losses are calculated by applying a dynamic energy balance under the transient regime.

The facility is based on a nine-year-old on-campus field with 50 m^2 flat plate solar collectors, which operated for a domestic hot water (DHW) application. The working parameters were recorded during an entire year for periods of 10 minutes. The model was experimentally validated by comparing its results to the instant collector temperatures and heat fluxes that were obtained from the experimental database.

Both of the experimental and model results were compared to the direct application of the collector efficiency normalization curve (ENC) that was obtained from the EN-12975:2006 test as a reference. Being the operating conditions unlike, differences throughout the day became evident. The influence of several factors is fully described in Part II of this paper.

Keywords: Solar energy; Flat plate collector; Transient model; Collector thermal efficiency; Collector performance; Solar Domestic Hot Water.

NOMENCLATURE:

A: Collector aperture area [m^2]

a_1: Collector efficiency normalization curve constant [W m^{-2} K^{-1}]

a_2: Collector efficiency normalization curve constant [W m^{-2} K^{-2}]

C_p: Specific heat [J Kg^{-1} K^{-1}]

c: EN12975:2006 collector efficiency constant

E_L: Long wave irradiation [W m^{-2}]

F´: Collector efficiency factor [-]

G: Solar irradiance [W m^{-2}]

H: Collector length slope-wise [m]

I: *INERTIA*: Thermal inertia [W]

K_θ: Incident angle modifier constant [-]

k_T: Clearness index $k_T = \frac{G_z}{G_o}$ [-]

L: Collector width [m]

m: Mass [kg]

Nu_H: Nusselt number for the wind normal component $Nu_H = \frac{h_H H}{K_{air}}$ [-]

Nu_L: Nusselt number for the wind parallel component $Nu_L = \frac{h_L L}{K_{air}}$ [-]

Pr: Prandtl number [-]

Pv: Partial pressure of water vapor in the ambient wet air [Pa]

Q: Heat power [W]

q: Fluid flow [m^{3}s^{-1}]

R: Thermal resistance [K W^{-1}]

Ra: Rayleigh number [-]

Rb: Ratio of the beam irradiance to horizontal total irradiance $Rb = \frac{\cos\theta}{\cos\theta_Z}$ [-]

Re_H: Reynolds number for the wind normal component $Re_H = \frac{\rho_{air}(u \sin[\xi]\, H]}{\mu_{air}}$ [-]

Re_L: Reynolds number for the wind parallel component $Re_L = \frac{\rho_{air}(u \cos[\xi]\, L]}{\mu_{air}}$ [-]

T: Temperature [K]

t: Time [s]

u: Wind velocity [m s^{-1}]

V: Volume [m^3]

ABBREVIATIONS:

DHW: Domestic Hot Water

ENC: Efficiency Normalization Curve

IAM: Incident Angle Modifier

GREEK:

α: Absorptance

ε: Emissivity

η: Efficiency

θ: Solar irradiance incident angle

ξ: Wind direction relative to the east to west direction

ρ: Density [kg m^{-3}]

σ: Stefan-Boltzmann constant [W m^{-2} K^{-4}]

τ: Transmittance

SUBCRIPTS:

0: Collector optical efficiency

a: Ambient

abs: Absorber plate

box: Box back surface of flat plate collector

cd: Convective at the collector, downwards

co: Collector

cint: Convective inside the collector

cup: Convective at the collector, upwards

d: Downwards

en: Effective in the collector normal direction

Ext: External

glass: Glass cover of the flat plate collector

inco: Collector inlet

ins: Insulation

int: Internal

m: Mean value between the collector inlet and the outlet temperatures

o: Extraterrestrial irradiance

outco: Collector outlet

rad: Radiation

sky: Sky

solar: Solar irradiance

up: Upwards

useful: Instantaneous useful power

w: Water

z: Total irradiance on the horizontal plane

B: Beam

D: Diffuse

EXP: Experimental

EXT: External

H: Based on the collector length slope-wise

INT: Internal

IR: Infrared

L: Based on the collector width

MOD: Model

NC: Efficiency Normalization Curve

T: Sloped plane

Z: Horizontal plane

1. INTRODUCTION

Solar irradiance is transformed inside of a collector into useful thermal energy, and this process results in an increased temperature of the inside flow. The energy conversion efficiency depends on the collector optical and thermal losses. These losses are due to the conduction, convection and radiation heat transfer processes to the environment and also to the local irradiance conditions and the collector optical properties, [1].

To characterize the collector performance, there are different testing standards for specific operating conditions, such as the ASHRAE-93 [2] and EN-12975 [3], which are enforced in the USA and European Union countries, respectively.

The ASHRAE-93 standard [2] requires an experimental determination of the steady-state collector efficiency under prescribed environmental and operating conditions for a range of collector fluid temperatures [4]. This standard describes how to determine the value of the collector incident angle modifier (IAM) at 0, 30, 45 and 60 degrees, which is required when the incident irradiance is not perpendicular to the collector surface.

On the other hand, the EN-12975 standard [3] allows testing the flat plate collector either in steady-state or in quasi-dynamic regimes, which offers an alternative for relaxing the environmental conditions that are required to fulfill the test. In this standard, the collector IAM is only calculated for an angle of 50 degrees, [4]. For the quasi-dynamic test, the EN-12975 standard [3] takes into account the thermal losses due to radiation, the convection from wind and the effective thermal inertia. Equation (1) shows a functional expression in which the test results are given for the quasi-dynamic normalization test.

$$\frac{Q_{useful}}{A} = F'(\tau\alpha)_{en}K_{\theta B}(\theta)G_B + F'(\tau\alpha)_{en}K_{\theta D}G_D - c_6 uG - c_1(T_m - T_a) - c_2(T_m - T_a)^2 - c_3 u(T_m - T_a) + c_4(E_L - \sigma T_a^4) - \quad (1)$$

Equation (1) allows calculating the useful heat obtained in the collector as a function of both the optical and thermal parameters. However, this detailed description is generally not available. Typically, the test reports offer only a function in terms of $\frac{(T_m - T_a)}{G_T}$ for the efficiency normalization curve (ENC), obtained under steady-state operating conditions. This will be used, as a reference, to later describe the ENC of the collector that was used in this work, the Vitosol 100 w2.5 by Viessmann Werke GmbH and Co KG®.

Rojas *et al.* [4] compared both of the USA and European standards experimentally and concluded that they end up in similar values of the ENC of a flat plate collector.

Related to the goal of describing the collector efficiency experimentally, several studies have been performed and have provided insight into the processes that are involved: [5] to [11]. As in the EN 12975 standard [3], the ASHRAE-93 standard [2] requires strict

environmental conditions to perform the test. Because of this, researchers have investigated different testing methods to allow the conditions to be more flexible and to increase the number of suitable days for testing. Approximately ten different methods to predict the collector performance under transient conditions were identified in the cited references. The respective authors classified them into four methods: simple, multi-node, multi-test and response function methods. The “simple methods” introduce the terms of thermal capacitance and separate the IAM for beam and diffuse irradiance components, [6], [12], [13], and others. The “multi-node methods”, such as those in [14] and [15] model up to four components in the collector: the glass cover, the thermal fluid, insulation, and the absorber plate. However, only one or two of the components are typically taken into consideration. The “multi-test methods”, such as those in [16] and [17], require the use of several tests to describe each collector performance parameter. They perform the tests under specific operating conditions, such as very high flow rates, which are not similar to the real working conditions of the collector. The “response function methods”, such as those in [18] and [19], are based on an impulse function that requires a large database.

Generally, solar collector performance has been modeled by using the Hottel-Whiller steady-state equation, which calculates the useful heat from an overall heat loss coefficient U in a similar manner to the above cited ENC, [1]. Some researchers have modified this equation to account for the thermal capacitance such that an approach to Equation (1) is performed. However, these authors were using what they call “the effective capacitance”, which is only the capacitance that considers the fluid together with the absorber plate, e.g., [14] and [15]. Using this method, “the effective capacitance” is related to the water temperature variations through coefficients that

empirically adjust for each component. In the present work, a different temperature and its variation will be considered for each component.

Furthermore, relevant studies have observed the performance of thermal solar facilities operating under steady-state or transient conditions by using experiments and/or simulation methods. These studies require a description of the collector operation. If the collector performance is more accurately implemented, then the model will estimate the behavior of the entire solar facility more precisely. The transient models address the importance of accounting for the thermal inertias and the time-varying environmental conditions around the collector to accurately predict its thermal losses, e.g., [20].

There are many renowned computer programs used for predicting the performance of solar facilities, such as TRNSYS [21], MINSUN [20] to [23], WATSUN [24] and others. These programs require meteorological data that was either generated by model based time-series synthesizers that use long term databases, such as METEONORM, TMD, TMY [25] or any other specific database for the region where the simulation is performed, such as DRY for Denmark, [26]. Meteorological data are typically given for mean hourly, monthly or annual periods. To obtain more accurate results, the simulation codes may require a smaller time step, and consequently, interpolated data should be generated, e.g., [25] and [27]. Nevertheless, it is a common practice to apply the ENC to characterize the collector performance even working under transient and low irradiance conditions, out of the standard operation window, as it is currently the only available information regarding performance of the collector. As Lecuona *et al*. [28] describe, several authors have developed procedures to incorporate the flow rate effects and other

variables into the ENC in an approximate manner, but they did not consider the thermal inertia.

Some researchers have shown the advantage of using actual meteorological data from the location where the solar facility was installed jointly with the instant yield of the facility. As a result, if the same inputs are used, then the comparison of the experimental performance of the collector to the simulation output is of a higher quality. With this philosophy Andersen and Furbo [26] compared the experimental data of a combi-system, for both solar DHW and heating, to the results of a TRNSYS simulation program.

The present work is part of a wider study that aims to model an entire solar facility that is used for DHW application under real working conditions, as seen in Figure 1. As part of this study, this paper describes the collector performance under transient conditions by representing each of the collector components as thermal resistances and thermal capacitances, in a similar way to the proposed in [36]. To predict the outlet collector temperature, the model requires input data such as the actual meteorological data as well as the inlet collector temperature and flow rate. Once the collector efficiency was obtained from the model, it was then validated with the experimental performance of the solar facility working under the different conditions throughout the observed year. In a first step, the goal was to verify whether the model results follow the daily and seasonal transient operation performances, and if the results accurately describe the collector efficiency under those transient working conditions.

The instantaneous experimental and model collector efficiency were then compared with the ENC. Noting that real working conditions were different from the operating

conditions that were used to obtain the ENC. Any significant difference was detected as seen in Figure 11 for 2008-09-14 (sunny day), indicating that not always ENC is able to describe the collector performance under real operating conditions.

In a second step, an important goal is to describe the most relevant factors that are responsible of the differences between the experimental and the ENC efficiency curves. These differences allow detecting and including the suitable modifications on the ENC predictions that should be incorporated to get a higher accuracy, depending on the specific working characteristics of the collector (wind velocity and direction, collector aging, etc).

Additionally, it is important to be able to describe the transient collector performance throughout the whole daytime, with the aim of having a right solar facility design and use, as well as the control protocols applied to it.

Solar cooling is an application example where a more accurate description of collector instantaneous performance is required. A direct drive of the cooling system, as Lecuona *et al*. [28] show, seems convenient, taking place thermal storage in the cooled side, or eventually by an internal chemical storage. In both cases, the transient aspects are decisive in the interaction between the collector and the absorption machine, with significant impact on the overall performance.

Part II of this paper describes in more detail the influence of different factors such as aging, wind velocity, IAM, thermal inertia and radiation losses.

2. TRANSIENT BEHAVIOR: BASIC PARAMETERS

A variable, important to describe the collector performance, is the incident solar irradiance at the collector sloped aperture area (G_T). Typically, this variable is calculated from the measured global horizontal irradiance by applying the isotropic sky model, as the EN-12975 standard [3] suggests.

Meteorological stations usually measure the global solar irradiance in a horizontal plane. To calculate G_T, the irradiance should be distributed into beam, diffuse and ground reflection components. Many researchers have studied the relationship between k_T and the diffuse irradiance component by using hourly data over several years, such as [29] to [32]. Vázquez and Santos [33] gave a correlation for k_T and the diffuse fraction of irradiance for a one-minute time period for Vigo, which is a city located in Northern Spain. In [34], the authors demonstrated the sensitivity of these types of correlations to the month of the year, i.e., to the declination angle of the Sun. These influences must be considered to accurately predict G_T, especially for periods of low irradiance such as the winter season. During this season, the contribution of the diffuse irradiance component is a higher fraction. Figure 2 shows a comparison between the results of the irradiance model applied with the legend “G Vázquez one min+seasonal” and the experimental data obtained from a Class 1 pyranometer, which was oriented with the same slope and surface azimuth angle as the flat plate collector field. The results are good and serve to validate the sky model. In Figure 2, the models described in [29] to [33] predict a lower global irradiance than that of the experimental results because they included a higher diffuse fraction of irradiance for the winter season.

The collector absorbs only a portion of the solar irradiance due to the optical properties of the glass cover and absorber plate, which are described in the $(\tau\alpha)_{en}$ and the IAM parameters for each irradiance component. The incidence angles for the diffuse and ground reflection are used as they were defined in [1]. The actual $(\tau\alpha)_{en}$ for the nine-year-old collector field under consideration was experimentally calculated, and the resulting value was 0.76. The IAM constants were provided by the solar collector manufacturer.

$$K_{\theta_B}(\theta_B) = 1 - 0.162\left[\frac{1}{\cos\theta_B} - 1\right] \quad (2)$$

$$K_{\theta_D}(\theta_D) = 1 - 0.221\left[\frac{1}{\cos\theta_D} - 1\right] \quad (3)$$

Thanks to a meteorological station on a tower that is six meters above the flat roof mounted collector field, this work uses local meteorological data for the horizontal irradiance, wind velocity and direction in a horizontal plane, ambient temperature and relative humidity. The sky temperature was calculated from *Ta*, k_T and *Pv*, following [35].

Table 1 shows in detail the dimensions and the thermal properties of each component of the collector. Additionally, the measured flow rate passing through the collector and the inlet temperature of the fluid were required to evaluate the thermal inertia of the components.

3. HEAT LOSS MODEL UNDER TRANSIENT CONDITIONS

Figure 4 shows the thermal circuit layout that was used to calculate the heat fluxes in the collector. The main heat flux heats the water flow inside the serpentine tube, which

is called the useful heat. Some of the heat is lost to the environment through the glass cover and through the collector box back surface, and hereafter this process is considered to be one-dimensional. The lateral thermal loss of the collector is negligible because the laterals were insulated and the absorber plate did not touch these surfaces. The heat loss through the glass cover is divided into radiation and convection. Radiation loss is not considered at the box back surface because the temperature of this surface is close to the temperature of the surrounding surfaces.

The thermal losses from the collector are divided into two terms as follows: From the absorber plate to the upper side: a) Convective loss due to free convection in the layer of air between the absorber plate and the parallel glass cover, b) Radiative loss between the absorber plate and the glass cover, c) Conductive loss across the glass cover, d) Radiative loss between the glass cover and the sky, e) Buoyancy-driven free convection and forced convection at the glass cover of the collector due to wind. From the absorber plate to the box back surface: a) Conductive loss across the insulation and the box back surface formed by aluminum sheet, and b) Buoyancy-driven free convection and forced convection at the box back surface.

These losses define the 18 elements in the thermal circuit, which is similar to the circuit that [36] describe. As shown in Figure 4, the thermal resistances are the circuit elements that represent the collector component through which heat fluxes travel; additionally, there are thermal capacitances that represent the thermal inertia of each of the collector components.

With the goal of calculating the thermal resistances of the collector model, small thermocouples were installed in contact with the representative surfaces (the glass cover

and the box back surface external sides and the absorber plate) as shown in Figures 1 and 3. Special care was taken to isolate the effects of solar irradiance and heat transfer through the thermocouple wire, which are both detrimental to the measurement accuracy. These measurements serve to obtain the elements of a thermal circuit based on resistances and capacitances, as shown in Figure 4.

The experimental facility from which the data were taken was composed of 50 m^2 of flat plate collectors facing south with a surface azimuth angle of 11 degrees east and a slope of 40 degrees, which corresponds to the local latitude. The collector field was located on a four-story building horizontal terrace in four rows that contained six, six, five and three collectors each.

3.1 Thermal resistances

In this work, the thermal circuit resistances related to conduction are obtained from the component material properties and dimensions, whereas for the convective resistances determination the collector components experimental temperatures on glass cover, box back surface and absorber plate have been measured on the solar facility during real operation.

The collector that was instrumented with the additional thermocouples corresponds to the third one in the row with five of them, as seen in Figure 1. A more detailed description of the solar facility can be found in [37].

As the thermal resistances R_{ins} and R_{int} depend mainly of the dimensions and the materials of the components of the collector, the heat fluxes coming from the absorber

plate to the upper (Q_{up}) and lower (Q_d) surfaces of the collector are experimentally determined by the direct measurement of the temperatures T_{abs}, T_{glass} and T_{box}.

This is especially clear in the case of R_{ins}, where conductive heat transfer through the insulation glass fiber is the dominant mechanism of the heat transfer.

Relative to R_{int}, due to the existence of natural convection (R_{cint}) and radiation (R_{rad_int},), a less precise determination of the upper heat flux was possible. To this point, the correlations for natural convection over and under inclined surfaces from [38, 39] were tried to describe the collector operation under no wind conditions. None of the usual correlations for natural convection inside rectangular cavities gave good results for the layer of air between the absorber plate and the parallel glass cover. The inhomogeneity of temperature along the absorber plate and its time evolution during the day are postulated as the responsible causes of the unsatisfactory results of R_{cint}, as can be seen in Figure 5. Because of that, a specific correlation for this layer of air was derived, once the experimental heat flux that crossed it was determined from the thermal balance and both temperatures T_{abs} and T_{glass} were measured. As can be seen in Figure 5, the Duffie correlation is able to describe the thermal resistance during midday hours but early in the morning and late in the evening the description is not accurate enough to give a satisfactory result in the energy balance. The global energy balance in the collector was used as a test of confidence for the derived heat fluxes.

Once the heat fluxes were determined, the convective and radiative heat transfer coefficients for the upper and the lower surfaces were derived from T_{glass}, T_{box}, T_a and T_{sky}. Those are shown in Equations (4) to (7) and (8) using the usual non-dimensional relationships among Nusselt, Reynolds and Prandtl numbers. It should be noted that those expressions are not intended to be applied as a general correlation for convective

heat transfer around solar collectors, because the specific characteristics of a solar plant, such as collectors' location and arrangement, have to be taken into consideration. Here the emphasis is placed on the combination of parallel and cross flow to obtain a global heat transfer coefficient under windy conditions for different wind directions.

3.1.1 External convection

To establish the influence of the wind direction, the external forced convection resistance to ambient (glass cover and box back surface) was calculated by selecting the experimental data that belong to the parallel and normal wind drafts with respect to the collector glass cover within an interval of ±10 degrees. Only the parallel wind component coincides with the one that the EN 12975 test describes. Nonetheless, the objective of this work is to obtain a description of the collector under real working conditions; therefore, the wind drafts will have arbitrary directions. The empirical correlations for *Nu* that were obtained for each of the surfaces in terms of *Re* and *Pr* are shown in Equations (4) to (7) for the respective direction selecting the suitable data, being the wind velocity measured with the anemometer located in the meteorological tower. These correlations were not obtained under laboratory test operating conditions but under real working conditions throughout a year.

$$Nu_{d_H} = 2{,}085 Re_H^{0.484} Pr^{\frac{1}{3}} \quad (4)$$

$$Nu_{d_L} = 71{,}21 Re_L^{0.194} Pr^{\frac{1}{3}} \quad (5)$$

$$Nu_{\perp p_H} = 1{,}109 Re_H^{0.526} Pr^{\frac{1}{3}} \quad (6)$$

$$Nu_{\perp p_L} = 17{,}258 Re_L^{0.325} Pr^{\frac{1}{3}} \quad (7)$$

The results show a similar tendency to the expressions that are used in the existing literature, as seen in Figure 6 A. Having segregated correlations for parallel and cross flow, allows including in the model the influence of wind direction.

The forced convective heat transfer coefficients are combined with the free convective heat transfer coefficients. Those are calculated following the indications in [38] and [39] for the glass cover and the box back surface, respectively. These free convective heat transfer coefficients were only applied if $\frac{Gr_L}{Re_L^2} \gg 1$.

The convective heat transfer coefficients that were calculated for each of the external surfaces, box back surface and glass cover, by applying the previously described equations, are shown in Figure 7.

Figure 6 A compares the convective heat transfer coefficients that were calculated by the model to a selection of the heat transfer coefficients that were available in the open literature versus the wind velocity, which was measured with the anemometer located in the meteorological tower. The correlations given above were also calculated using this wind velocity. The output of this part is a global convective heat transfer coefficient, noting that this wind velocity was not near the collector external surfaces but due to the atmospheric free flow (commonly given by the meteorological databases), as the former would require a more complex implementation. If the wind velocity near to the collector surfaces were used, each surface would have a different wind direction and magnitude due to the wind interaction with the collector rows and the building envelope. In Figure 6 A, only the convective heat transfer coefficient that was obtained for the glass cover is compared to correlations that were found in the open literature. The small loss through

the box back surface makes a similar study irrelevant. The comparison shows dispersion, among other authors´ correlations, e.g., [40] to [46] of a comparable magnitude to the dispersion that was obtained in this study. It is noteworthy that the present measurements are for an actual solar collector that is located in a collector field.

3.1.2 Internal convection

The measured temperatures T_{abs} and T_{glass} were used to determine the internal natural convection correlation between the glass cover and absorber plate, obtaining Equation (8).

$$Nu_{INT} = 1.333\ 10^{-9} Ra_{INT}^2 - 4.553\ 10^{-6} Ra_{INT} + 1.004 \quad (8)$$

Figure 6 B shows a comparison between the applicable correlations of Nusselt and Rayleigh numbers that were found in the open literature, [1] and [47], and the correlation that was experimentally determined in this work. They exhibit different behaviors, which can be attributed to the temperature distribution along the absorber plate.

3.1.3 Radiation losses

The external radiant resistance was modeled as a heat flow between the glass cover homogeneous temperature and the sky temperature, as shown in Equation (22). The internal radiant resistance was modeled as a heat flow between the absorber plate and the glass cover, as shown in Equation (9):

$$R_{rad_{Int}} = \frac{\frac{1}{\varepsilon_{IR_{glass}}} + \frac{1}{\varepsilon_{IR_{abs}}} - 1}{\sigma A_{co}\left(T_{glass}^2 + T_{abs}^2\right)\left(T_{glass} + T_{abs}\right)} \quad (9)$$

3.2 Thermal inertia

Regarding the capacitances that represent the thermal inertias, they were modeled for each element as shown by Equation (10):

$$INERTIA = \sum_{j} V_j \rho_j Cp_j \frac{dT_j}{dt} \quad (10)$$

The justification of employing all of the collector components is because the water inertia represents only 30% of the total collector inertia.

3.3 Collector model

The collector model was assembled and the thermal losses were calculated by applying a dynamic energy balance under the transient regime using thermal resistances and capacitances as shown in Equations (11) to (22).

$$R_{ins}Q_D = T_{abs} - T_{box} \quad (11)$$

$$R_{cd}Q_D = T_{box} - T_a \quad (12)$$

$$R_{int}Q_{UP} = T_{abs} - T_{glass} \quad (13)$$

$$R_{int} = \left(R_{rad_{Int}}^{-1} + R_{cint}^{-1}\right)^{-1} \quad (14)$$

$$R_{cup}Q_{CUP} = T_{glass} - T_a \quad (15)$$

$$R_{rad_{Ext}}Q_{RAD} = T_{glass} - T_{sky} \quad (16)$$

$$Q_{UP} = Q_{SOLAR} - Q_D - Q_{USEFUL} - INERTIA \quad (17)$$

$$Q_{SOLAR} = G_{co}A_{co} \quad (18)$$

$$Q_{USEFUL} = \dot{q}_{col}\rho_W C_p(T_{outco} - T_{inco}) \quad (19)$$

$$Q_{CUP} = Q_{UP} - Q_{RAD} \quad (20)$$

$$INERTIA = \sum_i m_i C_{pi} \frac{dT_i}{dt} \quad (21)$$

$$R_{rad_{Ext}} = \frac{1}{\sigma \varepsilon_{IR_{glass}} A_{co} \left(T_{glass} + T_{sky}\right)\left(T_{glass}^2 + T_{sky}^2\right)} \quad (22)$$

Once the empirical correlations for the thermal resistances are known, the entire system of differential equations is advanced in time by applying an implicit Euler finite-difference scheme. The inputs that were used are as follows: the absorbed solar radiation (which considers $(\tau\alpha)_{en}$ and the IAM), the wind velocity and direction, the flow rate, the ambient, sky, and inlet temperatures. The model outputs were the temperatures of all of the collector components along with the outlet temperature and the useful heat and thermal losses.

The time step for the model and the measured variables coincide at 10 minutes. This time step allows for a good knowledge of the actual variations of all of the environmental conditions that were obtained, such as the solar irradiance and wind velocity. These instantaneous variations were especially important for the description of the experimental and model heat fluxes on cloudy days, as discussed in Section 4.

4. EXPERIMENTAL VALIDATION

The purpose of this part is to test if the collector overall heat loss obtained from the model coincides with the experimental collector heat loss within the variations of natural meteorology. The first one is based on convective and radiative heat transfer coefficients included in the model, explained in the preceding section, and the measured environmental data (ambient temperature, pressure and humidity, and irradiance). The second one is derived from experimental measurements (temperatures and flows).

The time period analyzed in this work was one year, from 2008-02-27 to 2009-02-26, a total of 144 data/day for each of the measured variables. The solar collector field pump operated each day for a period of 7 to 22 hours continuously moving a total water flow rate of 0.6 10^{-3} m^3 s^{-1} (0.3 10^{-4} m^3 s^{-1} per collector). This flow rate coincides with the flow rate from the Institut für Solartechnik SPF [49] that was used for the ENC determination.

According to the CTE 2006 (Spanish Code for building) [50], this facility could be suitable for a residential building of 47 apartments in Madrid satisfying the prescribed minimum of 60% of the DHW demand at 60ºC supply temperature.

The measurements of the ambient temperature, as well as the wind velocity and direction were performed in the proximity of the collector field, simultaneously with the rest of the measurements; in particular, for the absorber plate, glass cover and back cover temperatures. The distance from the wind velocity and direction sensors to the collector field is of the same order of magnitude than the collector field dimension itself; i.e. around 20 m.

The instrumentation, primarily the thermocouples for inlet and outlet temperatures and flow meters, were in-situ calibrated after their installation.

The results of a representative sunny day (2008-09-14) and cloudy day (2008-05-04) are shown in Figure 8. In both cases, the temperatures at the outlet and at the absorber plate were accurately described; meanwhile, the glass cover and box back surface temperatures did not match as precisely, which is primarily attributed to the simplifications of the model.

Regarding the heat fluxes in the collector, Figure 9 shows the useful heat and the upwards and downwards heat losses for the same representative sunny and cloudy days, their temporal evolution is accurately described. The average at the end of the sunny day is as follows: of the total incident solar energy, the useful heat is 64%, the heat loss through the glass cover represents 12%, the heat loss through the box back surface is 4%, the remaining 20% is for the optical losses. For the cloudy day data, the need for using a sufficiently small time step becomes evident for the accurate determination of the collector performance.

The calculation was repeated for each day of the one-year period that was considered. Figure 10 shows the resulting time evolution of the daily useful heat that was obtained from the model and the one that was calculated from the experimental temperatures and mass flow rate. A statistical analysis shows the average and dispersion (at 95% of probability) relative errors of 1.6% ± 27% around the instantaneous values. This small amount of error indicates that the yearly averages can be predicted with high accuracy.

5. RESULTS AND DISCUSSION

There are two different efficiencies, one obtained from experimental data, Equation (23), and another from the application of the model, Equation (24).

$$\eta_{EXP} = \frac{Q_{useful_{EXP}}}{G_T A_{co}} = \frac{\dot{q}_{co}\rho_w C_p (T_{outco} - T_{inco})}{G_T A_{co}} \quad (23)$$

$$\eta_{MOD} = \frac{Q_{useful_{MOD}}}{G_T A_{co}} = \frac{\dot{q}_{co}\rho_w C_p \left(T_{outco_{MOD}} - T_{inco}\right)}{G_T A_{co}} \quad (24)$$

For this specific collector the Institut für Solartechnik SPF [49] obtained the ENC applying the EN 12975 standard [3], which could be easily calculated:

$$\eta_{NC} = 0.85 - 4.07\left(\frac{T_m - T_a}{G_T}\right) - 0.0070 G_T \left(\frac{T_m - T_a}{G_T}\right)^2 \quad (25)$$

Figure 11 shows the three efficiencies for the sunny and the cloudy days chosen vs. the official time and the $\left(\frac{T_m - T_a}{G_T}\right)$ parameter. The model accurately describes the experimental efficiency; meanwhile, the ENC exhibits a dissimilar behavior. This is because the working conditions in this case are not the same. During the sunny day, the inertial effect causes a curvature in the collector efficiency curve in both the experimental and the model results. At midday, the efficiency reaches a maximum, and afterwards, the tendency is parallel to the collector ENC. The lower values are attributed to effects that are not taken into account by the ENC, such as aging, dust and wind losses [48].

Figure 12 shows the same three efficiencies for the evolution of the entire year. Only the time period when the solar irradiance was higher than 300 W m^{-2} is included for this case to eliminate the numerical inaccuracies on efficiency when G_T is small. The model follows the experimental efficiency reasonably well. At the same time, the differences between the experiment and the ENC were noticeable due to the effects that were previously discussed.

As seen in Figure 11, the ENC is not able to describe the time evolution throughout a day of the instantaneous solar collector efficiency. In this sense, a low correlation may be expected between experimental (and modeled) collectors' efficiency and the ENC efficiency. This way Figure 12 shows the whole population of measurements and derived parameters that were obtained from them throughout the whole year.

A detailed description is needed to explain the differences between the coinciding experimental and model efficiencies with the ENC in order to show the more influential parameters. The corrections that must be applied as a function of them are shown in Part II of this paper, [48].

6. CONCLUSIONS

The main conclusions obtained from the study are as follows:

- A model for the solar thermal collector under transient conditions, including the thermal inertia of each component, was performed and validated experimentally under actual outdoor working conditions. The model is able to describe the instantaneous heat production, being this relevant for applications where solar collectors are directly connected to the application, such as solar cooling.
- Correlations for the external and internal convection heat transfer coefficients were determined experimentally using the measurements of three surface temperatures.
- The correlations for the external convection heat transfer coefficients of the glass cover and box back surfaces were calculated by considering the angles between the wind and the collectors. A global heat transfer coefficient was obtained for both surfaces for a combination of the parallel and cross flows.
- For the flow between the glass cover and the absorber plate, a correlation for the free convection heat transfer coefficient was also experimentally obtained.
- The collector efficiency was calculated by using the experimental performance data and through the application of the model. These two results show very similar figures but lower than the collector simpler model of the ENC. Consequently, the ENC seems not suitable to accurately calculate the collector performance due to the fact

that real working conditions are significantly different than the normalization test operating conditions.

- The water inside of the collector represents a thermal inertia that is 30% of the total thermal inertia. The contribution to inertia of the other components of the collector, such as the glass cover, the absorber plate and the collector pipes, has been described and quantified. Their contribution must be considered in transient operations.
- To accurately determine the collector absorbed irradiance, the variation of the diffuse component of solar irradiance with the declination angle and the separate IAM constants should be considered.

ACKNOWLEDGMENTS

This work was partially funded by the Spanish government research grant M. C. T. CLIMABCAR project DPI 2003-01567, MINICON project (FIT 0204-2004-68 and FIT 020100-2003-233) and SACSCC (ENE 2007-63965). Their contribution is greatly appreciated.

REFERENCES

[1] Duffie, J. A., Beckman, W.A. 2006 Solar Engineering Thermal Processes. USA: John Wiley and Sons,

[2] ASHRAE-93:2003. Methods of testing to determine the thermal performance of solar collectors. Atlanta: ASHRAE.

[3] UNE:EN-12975:2006. Sistemas solares térmicos y componentes. Captadores solares. Madrid: AENOR.

[4] Rojas D., Beermann J., Klein S.A., Reindl D.T., 2008. Thermal performance testing of flat-plate collectors. Solar Energy 82, 746-757

[5] Amer E.H., Nayak J.K., Sharma G.K., 1997. Transient test methods for flat-plate collectors: Review and experimental evaluation. Solar Energy 60, 229-243.

[6] Perers B., 1997. An improved dynamic solar collector test method for determination of non-linear optical and thermal characteristics with multiple regression. Solar Energy, 59, 163-178

[7] Amer E.H., Jadeja P., Nayak J.K., Sharma G.K., 1998. Comparison of two dynamic test methods for solar flat-plate collectors. Energy Conversion and Management 39, 285-293.

[8] Amer E.H., Nayak J.K., Sharma G.K., 1998. Transient method for testing flat-plate solar collectors. Energy Conversion and Management 39, 549-558.

[9] Amer E.H., Nayak J.K., 1999. Evaluation of a transient test procedure for solar flat-plate collectors. Energy 24, 979-995.

[10] Amer E.H., Nayak J.K., Sharma G.K., 1999. A new dynamic method for testing solar flat-plate collectors under variable environmental. Energy Conversion and Management 40, 803-823.

[11] Nayak J.K., Amer E.H., 2000. Experimental and theoretical evaluation of dynamic test procedures for solar flat-plate collectors. Solar Energy 69, 377-401.

[12] Hawlader, M.N.A., Wijeysundera N.E. 1987 Solar collector testing. Renewable Energy Review Journal 9, 11-28.

[13] Sourproun, A.V. 1992 Dynamic method of solar collector testing. ASME J. Solar Energy Engineering, 2,: 1149-1154

[14] Kamminga, W. 1984 Experiencies of a solar collector test method using Fourier transfer functions. International Journal of Heat and Mass Transfer 28, 1393-1404.

[15] Kamminga, W. 1985 The approximate temperatures within a flat-plate solar collector under transient conditions. International Heat and Mass Transfer 28, 433-440.

[16] Chungpaibulpatana, S., Exell R.H.B. 1988 The effect of using a one node heat capacitance model for determining solar collector performance parameters by transient test methods. Solar Wind Technology 5,: 411-421.

[17] Chungpaibulpatana, S., Exell R.H.B. 1990 Transient method for testing flat-plate solar collectors. Energy and the Environment into the 1990´s. Oxford Pergamon Press,. 699-703.

[18] Emery, M., Rogers B.A. 1984 On a solar collector thermal performance test method for use in variable conditions. Solar Energy 33,: 117-123.

[19] Wang, X.A., Xu Y.F., Meng X.Y. 1987 A filter method for transient testing of collector performance. Solar Energy 38,: 125-134.

[20] Perers B., 1993. Dynamic method for solar collector array testing and evaluation with standard database and simulation programs. Solar Energy 50, 517-526

[21] Klein, S.A., Cooper P.I., Freeman T.L., Beekman D.M., Beckman W.A., Duffie J.A. 1975 A method of simulation of solar processes and its application. Solar Energy 17, 29-37

[22] Adsten M., Perers B., Wäckelgård E., 2002. The influence of climate and location on collector performance. Renewable Energy 25, 499-509.

[23] Hellstrom B., Adsten M., Nostell P., Karlsson B., Wäckelgard E., 2003. The impact of optical and thermal properties on the performance of flat plate solar collectors. Renewable Energy 28, 331-344.

[24] Chandrashekar, M., Hollands K.G.T., Le N. T., Orgill J.F. 1978 WATSUN- A simulation program for solar assisted heating systems. Int. Renewable alternatives Proceedings of the Fourth Annual Conference. London, Ontario Canada.

[25] Remund, J. 2008 Chain of algorithms to compute hourly radiation data on inclined planes used in Meteonorm. Bookchapter of Modeling Solar Radiation at the Earth Surface, de V Badescu, 393-409. Berlin: Springer.

[26] Andersen, E., Furbo S. 2009 Theoretical variations of the thermal performance of different solar collectors and solar combisystems as function of the varying yearly weather conditions in Denmark. Solar Energy 83, 552-565

[27] Cuadros, F., López-Rodríguez F., Segador C., Marcos A. 2007 A simple procedure to size active solar Heating schemes for low-energy building design. Energy and Buildings 39, 96-104

[28] Lecuona A., Ventas R., Venegas M., Zacarías A., Salgado R. 2009 Optimum hot water temperature for absorption solar cooling. Solar Energy, Volume 83, Issue 10, October, Pages 1806-1814

[29] Collares-Pereira, M., Rabl A. 1979 The average distribution of solar radiation-correlations between diffuse and hemispherical and between daily and hourly insolation values. Solar Energy 22, 155-162.

[30] Erbs, D. G., Klein S. A., Duffie J. A. 1982 Estimation of the diffuse radiation fraction for hourly, daily and monthly average global radiation. Solar Energy 28, 293-302.

[31] Reindl, D.T., Beckman W.A., Duffie J.A. 1990 Diffuse fraction correlations. Solar Energy 45, 1-7.

[32] Mondol, J.D., Yohanis Y.G., Norton B. 2008 Solar radiation modelling for the simulation of photovoltaic systems. Renewable Energy 33, 1109-1120.

[33] Vázquez, M., Santos J.2004 Correlaciones minutarias, horarias y diarias de la radiación solar difusa a la radiación solar global en Vigo.» En Libro de Actas del XII Congreso Ibérico y VII Congreso Iberoamericano de Energía Solar, de M. Vázquez y José F. Seara, ISBN 1165-1170. International Solar Energy Society.

[34] Vázquez, M., Ruiz V., Perez R. 1991 The roles of scattering, absorption and air mass on the diffuse to global correlations. Solar Energy 47, 181-188.

[35] Aubinet, M. 1994 Longwave sky radiation parametrizations. Solar Energy 53, 147-154.

[36] Cristofari C., Notton G., Poggi P., Louche A., 2002 Modeling and performance of a copolymer solar water heating collector. Solar Energy 72, 99-112.

[37] Rodríguez Hidalgo, M.C., Rodríguez Aumente P., Izquierdo Millán M., Lecuona Neumann A., Salgado Mangual R., 2008 Energy and carbon emission savings in Spanish housing air-conditioning using solar driven absorption system. Applied Thermal Engineering 28, 1734-1744.

[38] Vliet, G.C. 1969 Natural convection local heat transfer on constant heat flux inclined surfaces. Transactions of the ASME Journal of Heat Transfer 91, 511-516.

[39] Churchill, S.W., Chu H.H.S. 1975 Correlating equations for laminar and turbulent free convection from a vertical plate. International Journal of Heat and Mass Transfer 18, 1323-1329.

[40] Watmuff, J.H., Charters W.W.S., Proctor D. 1977 Solar and wind induced external coefficients solar collectors. Comples 2, 56.

[41] Lunde, P.J. 1980Solar Thermal Engineering. New York: John Wiley and Sons.

[42] Test, F.L., Lessmann R.C., Johary A. 1981 Heat transfer during wind flow over rectangular bodies in the natural environment. Transactions of the ASME: Journal of Heat Transfer 103, 262-267.

[43] Kind, R.J., Gladstone D.H., Moizer A.D. 1983 Convective heat losses from flat-plate solar collectors in turbulent winds. Transactions of the ASME Journal of Solar Energy Engineering 105, 80-85.

[44] Sharples, S., Charlesworth P.S. 1998 Full-scale measurements of wind-induced convective heat transfer from a roof-mounted flat plate solar collector. Solar Energy 62, 69-77.

[45] Sartori, E. 2006 Convection coefficient equations for forced air flow over flat surfaces. Solar Energy 80, 1063-1071.

[46] Kumar S., Mullick S.C. Wind heat transfer coefficient in solar collectors in outdoor conditions. Solar Energy 2010 doi:10.1016/j.solener.2010.03.003

[47] Aounallah, M., Addad Y., Benhamadouche S., Imine O.,Adjlout L., Laurence D. 2007 Numerical investigation of turbulent natural convection in an inclined square cavity with a hot wavy wall. International Journal of Heat and Mass Transfer 50, 1683-1693.

[48] Rodríguez-Hidalgo, M.C., Rodríguez Aumente P., Lecuona A., Gutierrez Urueta G.L., Ventas R., Flat plate thermal solar collector efficiency: Transient behaviour under working conditions. Part II:Model application and design contributions. Applied Thermal Engineering, 2010.

[49] Institut für Solartechnik SPF Oberseestrasse 10 CH-8640 Rapperswil Switzerland SPF-Nr. C331 http://www.solarenergy.ch/ .

[50] Real Decreto 314/2006. Código Técnico de la Edificación. Boletín Oficial del Estado, BOE 28/03/06, 2006, Madrid, Spain.

Figure 1: View of the experimental solar collector field.

Figure 2: Experimental irradiance in the horizontal and sloped planes, measured with a Class 1 pyranometer vs. the official time in Spain (UTC/GMT +1 in winter and +2 in summer). Comparison among the different irradiances in the sloped plane, using the diffuse correlations given by several authors such as Collares-Pereira and Rabl 1979, Erbs *et al*. 1982, Reindl *et al*. 1990, , Vázquez *et al*. 1991, Vázquez and Santos 2004, Mondol *et al*. 2008. The data correspond to 2009-12-16, a representative sunny winter day.

Figure 3: Diagram showing the thermocouples added to the flat plate thermal collector and their insulating covers.

Figure 4: Equivalent thermal circuit. Thermal resistances and capacitances, measured temperatures and heat fluxes in the collector section.

Figure 5: Comparison among experimental, model and open literature correlations for the internal thermal resistance $R_{cint.}$

Figure 6: A. Comparison of convective heat transfer coefficient vs. wind velocity. B. Comparison of Nusselt number transfer coefficient vs. Rayleigh number.

Figure 7: A. Wind velocity magnitude and direction (0º from the east, clockwise) for 2008-03-20 vs. the official time. B. External convective heat transfer coefficient obtained from experimental data and model correlations for the glass cover. C. External convective heat transfer coefficient obtained from experimental data and model correlations for the box back cover.

Figure 8: Collector model and experimental temperatures vs. the official summer time in Spain (UTC/GMT+2h) for 2008-09-14 (sunny day) and 2008-05-04 (cloudy day).

Figure 9: Collector heat rate distribution vs. official summer time. Model validation with experimental heat fluxes for 2008-09-14 (sunny day) and 2008-05-04 (cloudy day).

Figure 10: Comparison between the daily useful heat obtained from the model and the heat calculated through the experimental temperatures and mass flow rate over a year. The auxiliary lines indicate the confidence interval as indicated in the text: 1.6% ± 27%.

Figure 11: ENC, experimental and collector model efficiencies vs. the official summer time and the $\left(\frac{T_m - T_a}{G_T}\right)$ parameter for 2008-09-14 (sunny day) and 2008-05-04 (cloudy day).

Figure 12: Collector efficiency. Experimental, collector model and normalization curve vs. $\left(\frac{T_m - T_a}{G_T}\right)$ parameter with a solar irradiance (G_T) threshold of 300 W m^{-2} over the entire year studied.

Table 1: Collector main parameters.

We developed and validated a transient model for a real thermal solar plant.

Heat transfer coefficients collector field were experimentally obtained.

Collector field performances far from the normalizing test conditions are predicted.

COLLECTOR PARAMETERS	
Collector width	2.390 m
Collector length	1.139 m
Aperture area	2.500 m^2
Absorber area	2.500 m^2
Glass cover thickness	4 mm
Inner air layer thickness	26 mm
Absorber sheet thickness (material: Cu)	0.25 mm
Serpentine exterior diameter (material: Cu)	10 mm
Insulation thickness (mineral fiber)	50 mm
Box back cover thickness (aluminum)	2 mm
ε_{IR_glass}	0.1
ε_{IR_abs}	0.1
Collector flow rate	0.6 10^{-3} m^3 s^{-1}

Table 1: Collector main parameters.

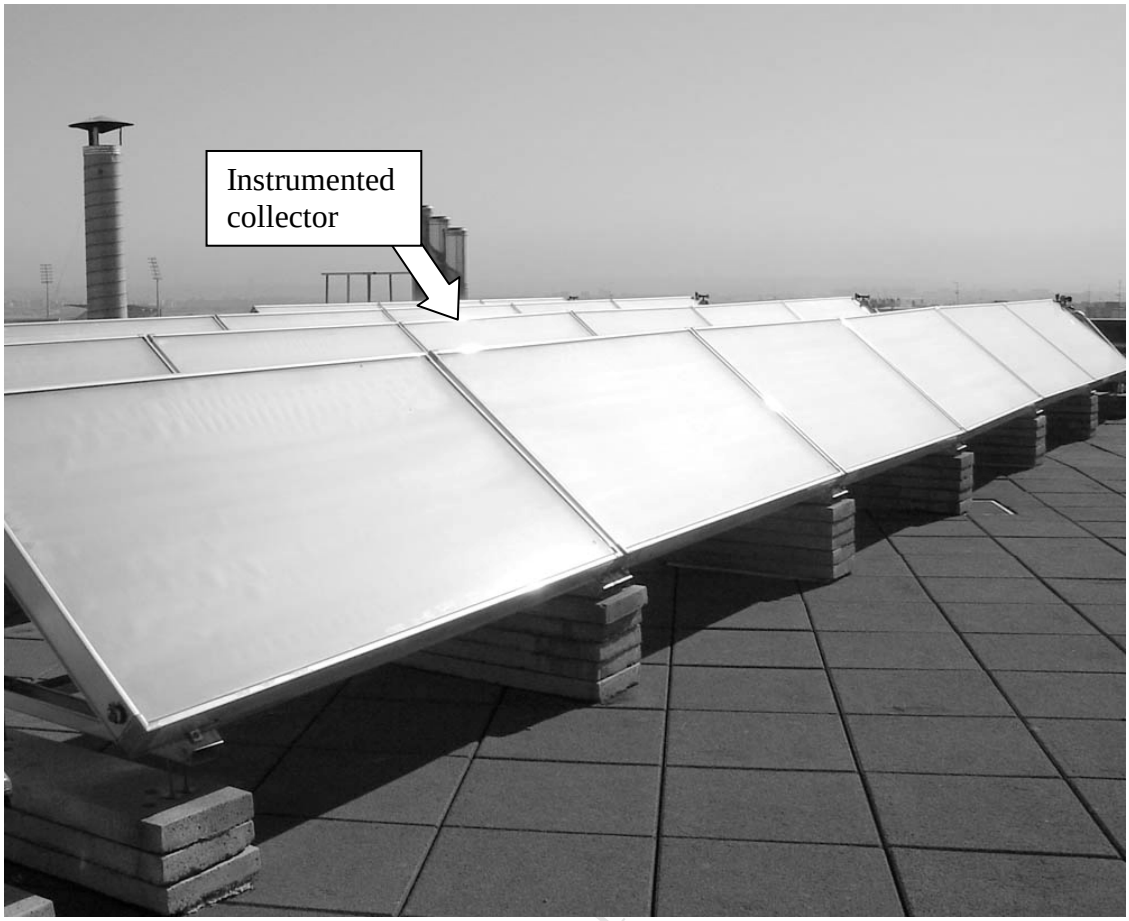

Figure 1: View of the experimental solar collector field.

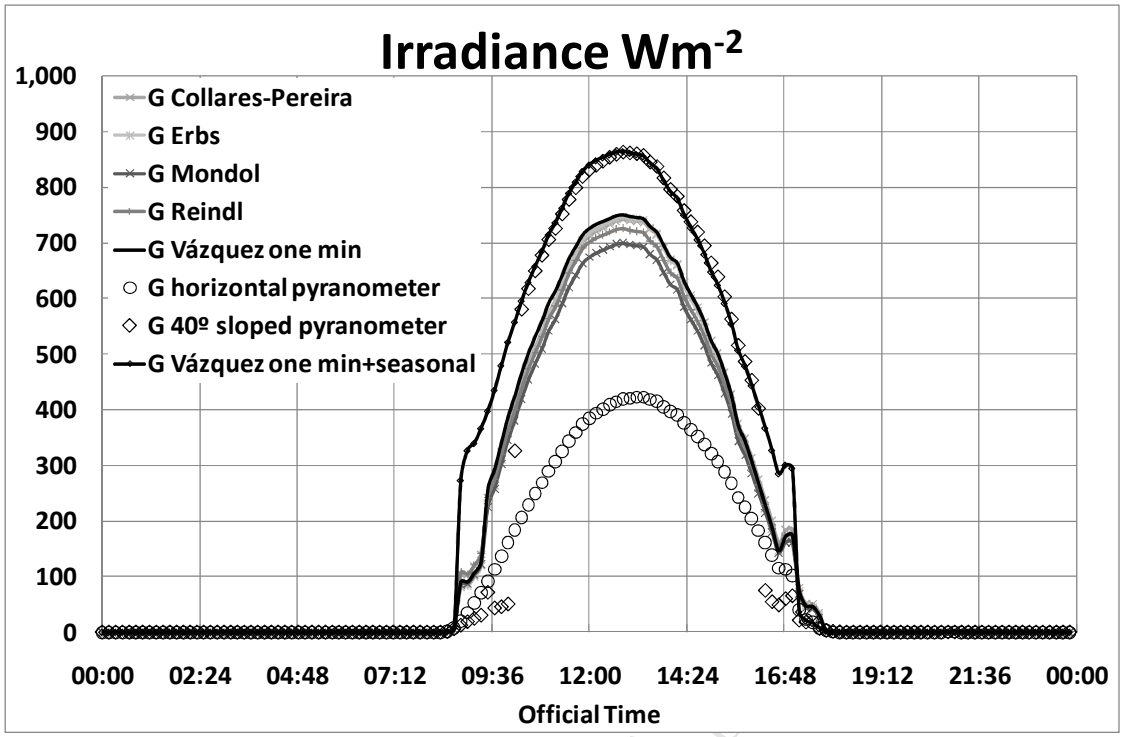

Figure 2: Experimental irradiance in the horizontal and sloped planes, measured with a Class 1 pyranometer vs. the official time in Spain (UTC/GMT +1 in winter and +2 in summer). Comparison among the different irradiances in the sloped plane, using the diffuse correlations given by several authors such as Collares-Pereira and Rabl 1979, Erbs *et al*. 1982, Reindl *et al*. 1990, , Vázquez *et al*. 1991, Vázquez and Santos 2004, Mondol *et al*. 2008. The data correspond to 2009-12-16, a representative sunny winter day.

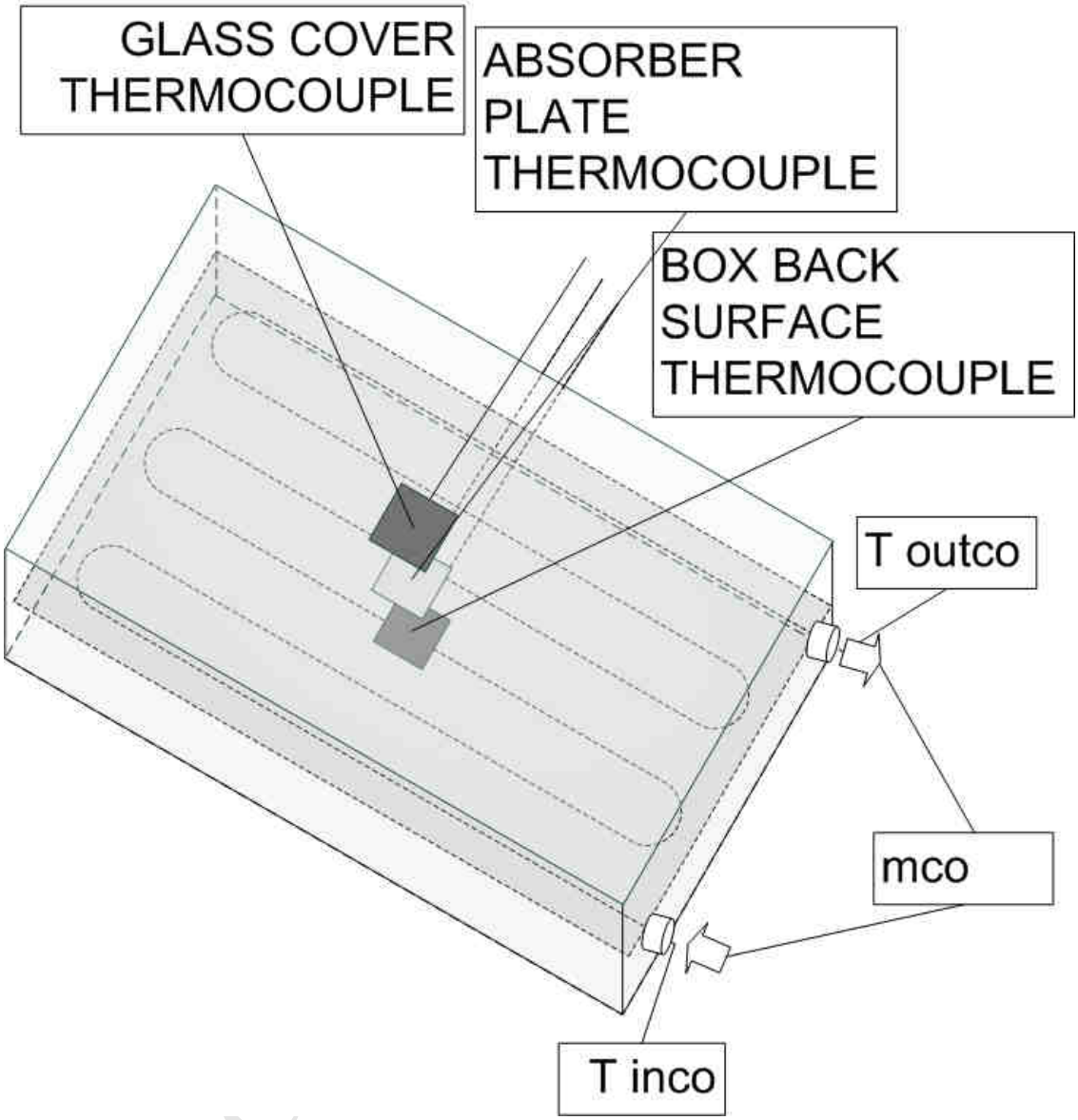

Figure 3: Diagram showing the thermocouples added to the flat plate thermal collector and their insulating covers.

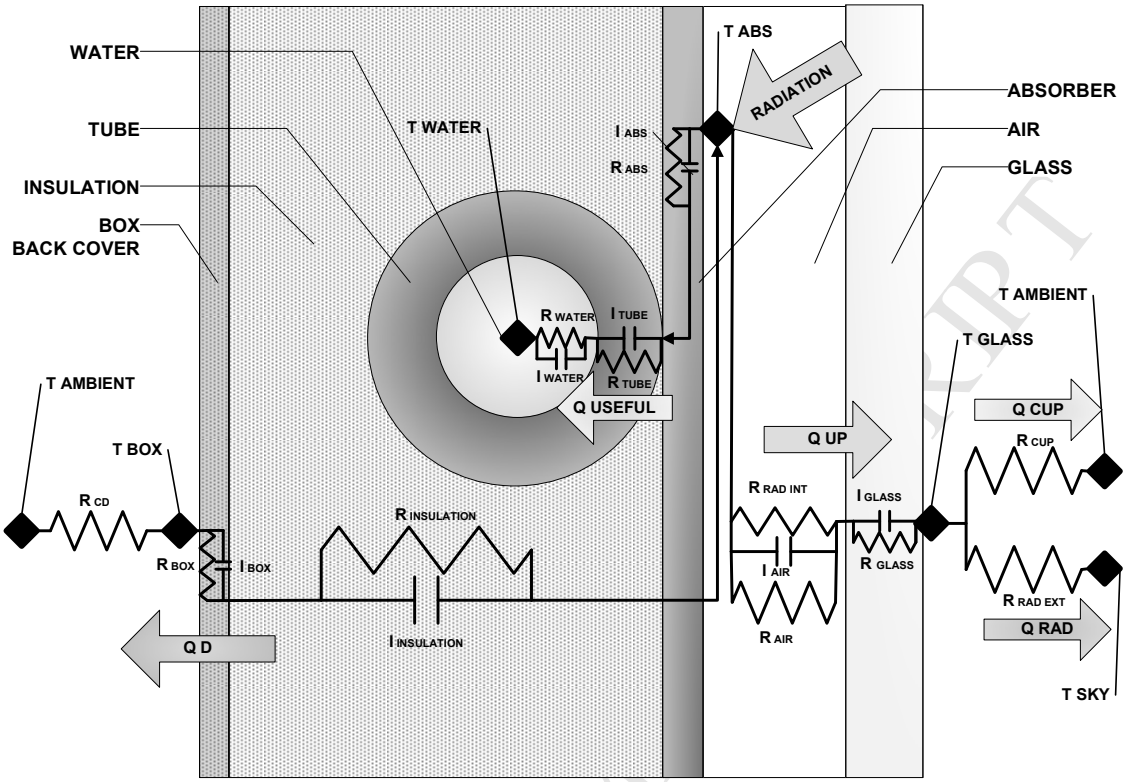

Figure 4: Equivalent thermal circuit. Thermal resistances and capacitances, measured temperatures and heat fluxes in the collector section.

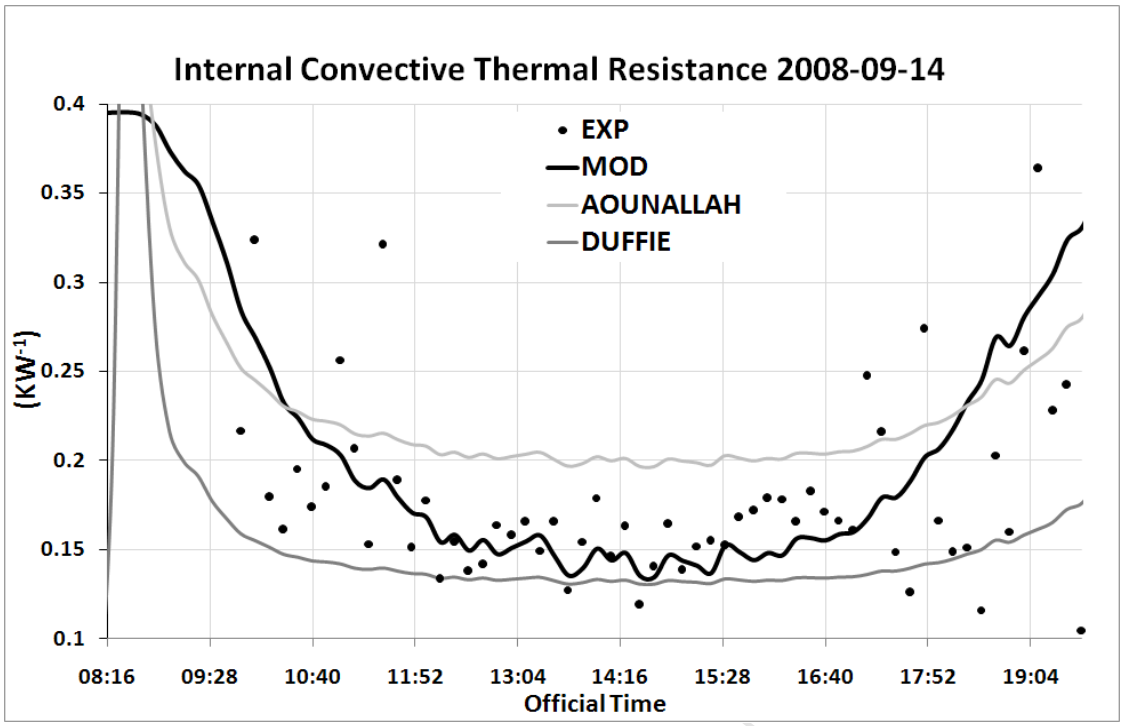

Figure 5: Comparison among experimental, model and open literature correlations for the internal thermal resistance R_{cint}

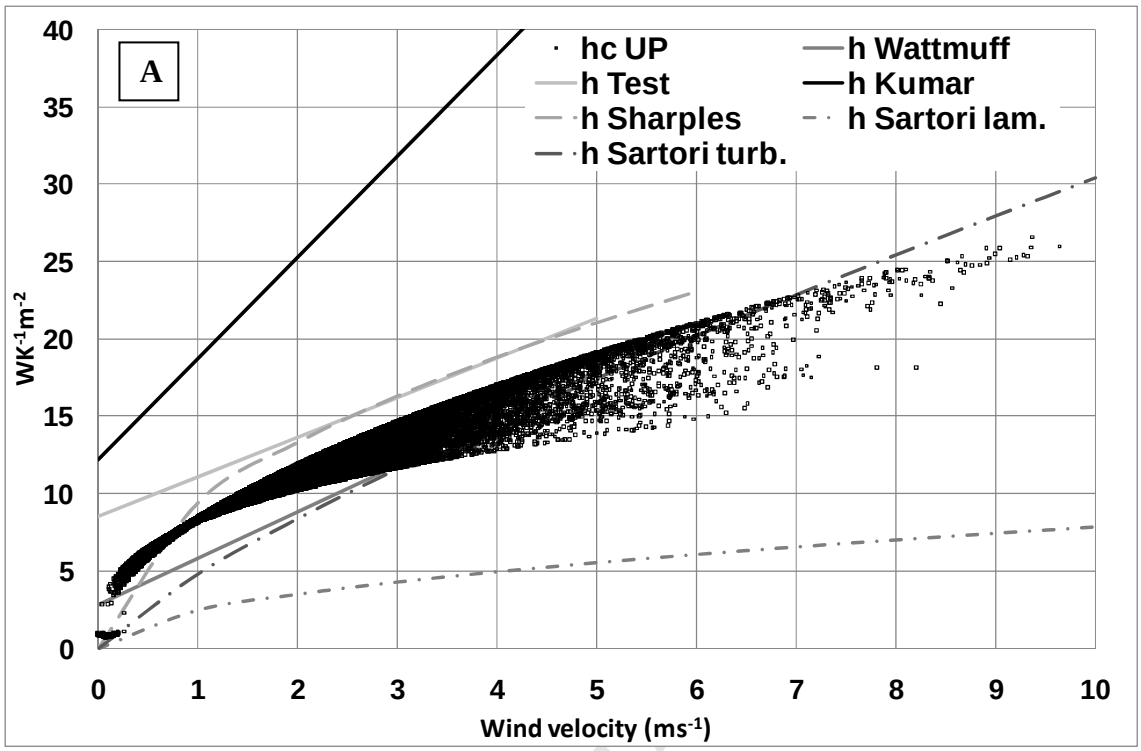

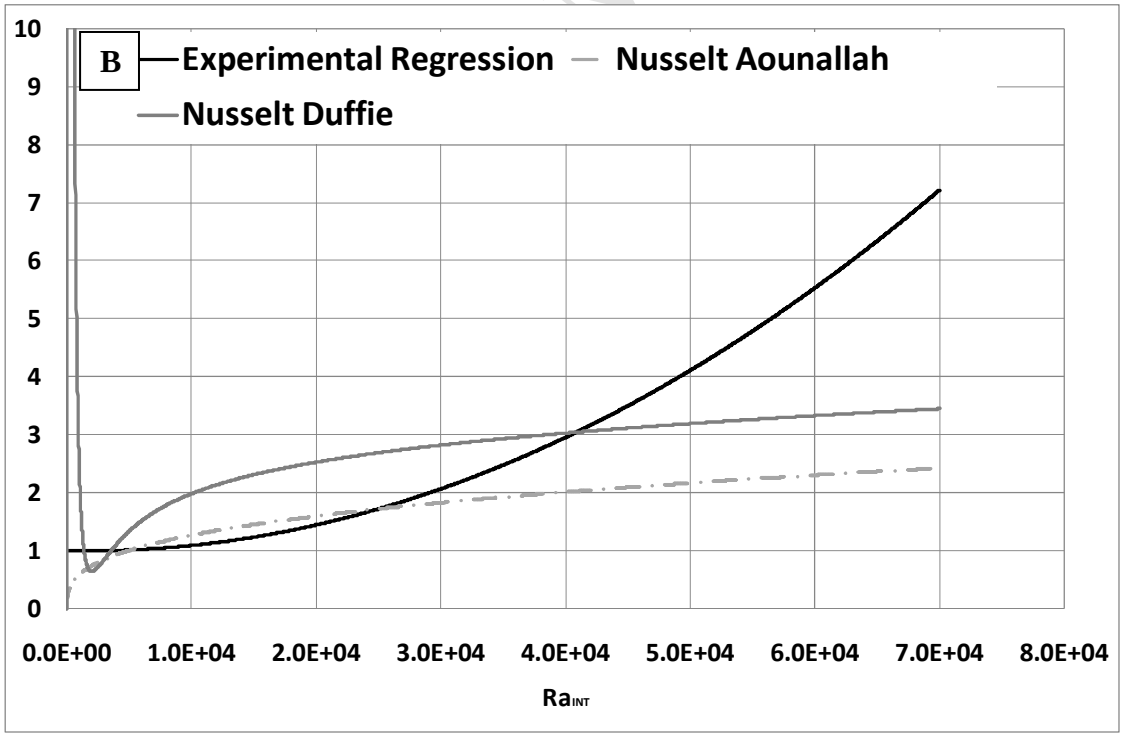

Figure 6: A. Comparison of convective heat transfer coefficient vs. wind velocity. B. Comparison of the Nusselt number vs. Rayleigh number for the layer of air between the absorber plate and the parallel glass cover.

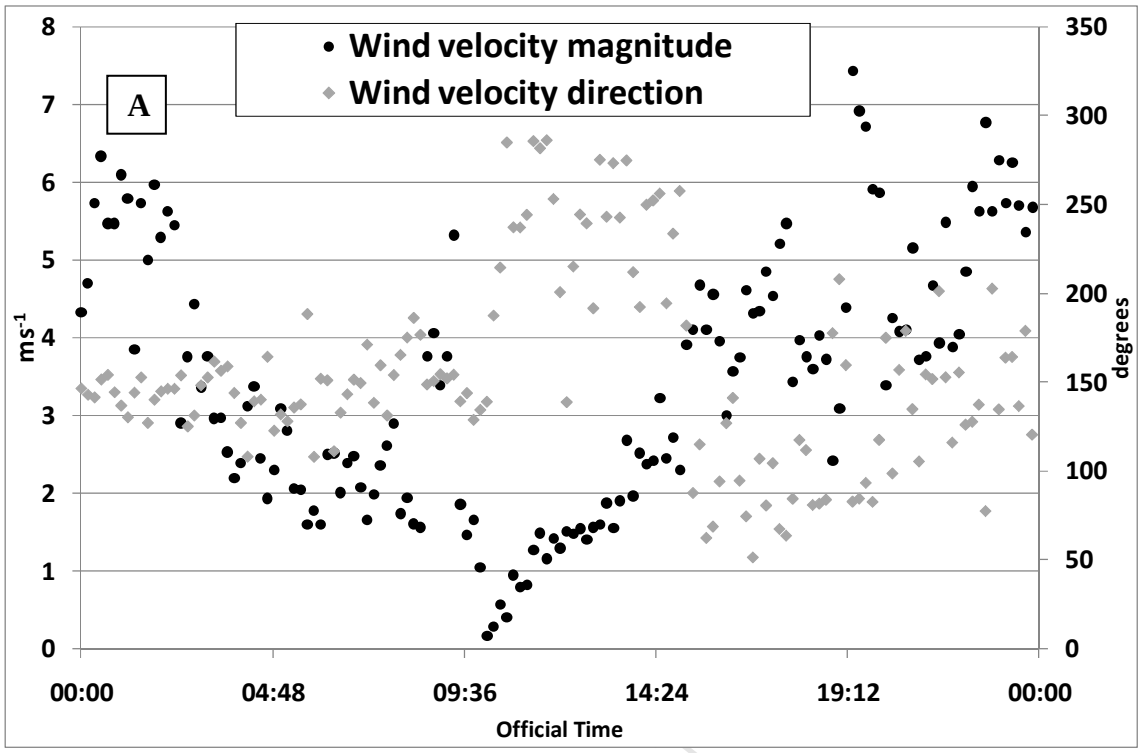
A
Wind velocity magnitude
Wind velocity direction
ms-1
degrees
0
1
2
3
4
5
6
7
8
0
50
100
150
200
250
300
350
00:00
04:48
09:36
14:24
19:12
00:00
Official Time

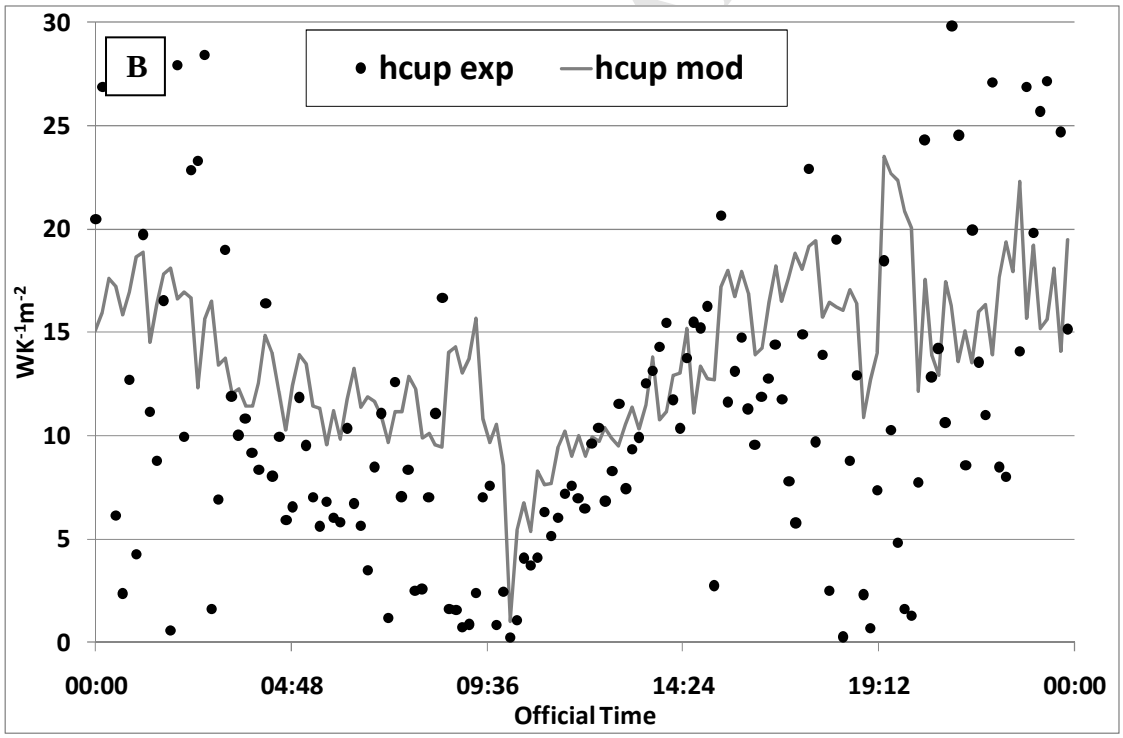
B
hcup exp
hcup mod
WK-1m-2
0
5
10
15
20
25
30
00:00
04:48
09:36
14:24
19:12
00:00
Official Time

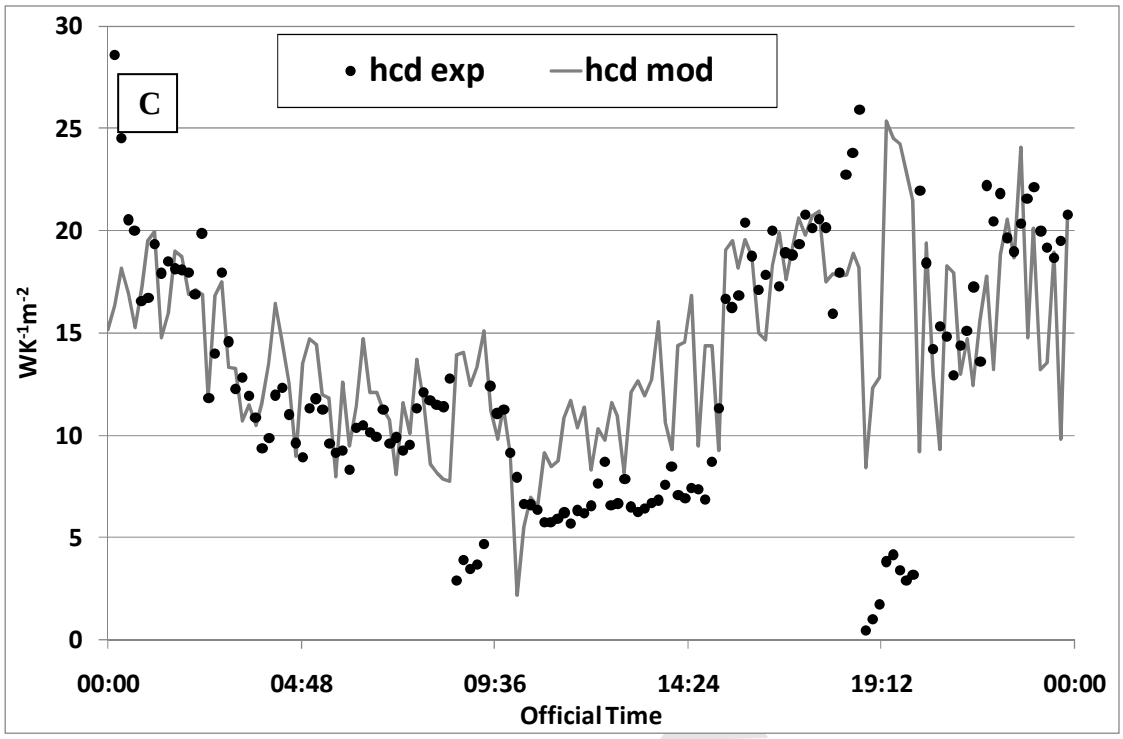

Figure 7: A. Wind velocity magnitude and direction (0º from the east, clockwise) for 2008-03-20 vs. the official time. B. External convective heat transfer coefficient obtained from experimental data and model correlations for the glass cover. C. External convective heat transfer coefficient obtained from experimental data and model correlations for the box back cover.

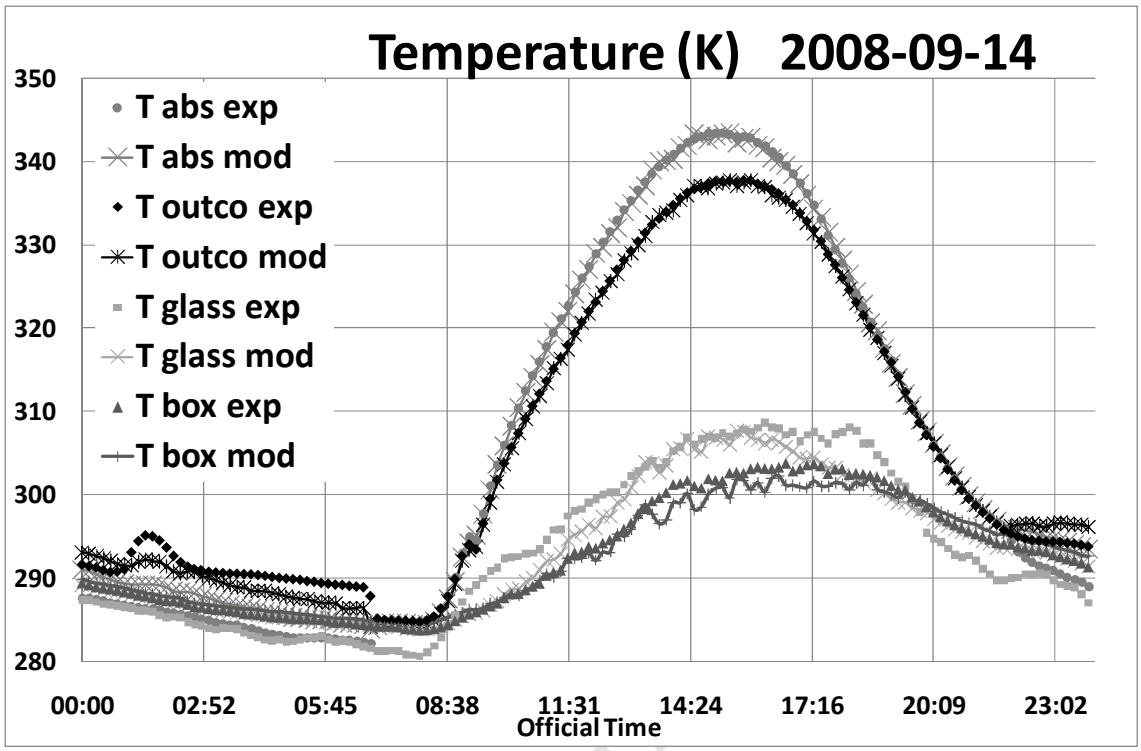

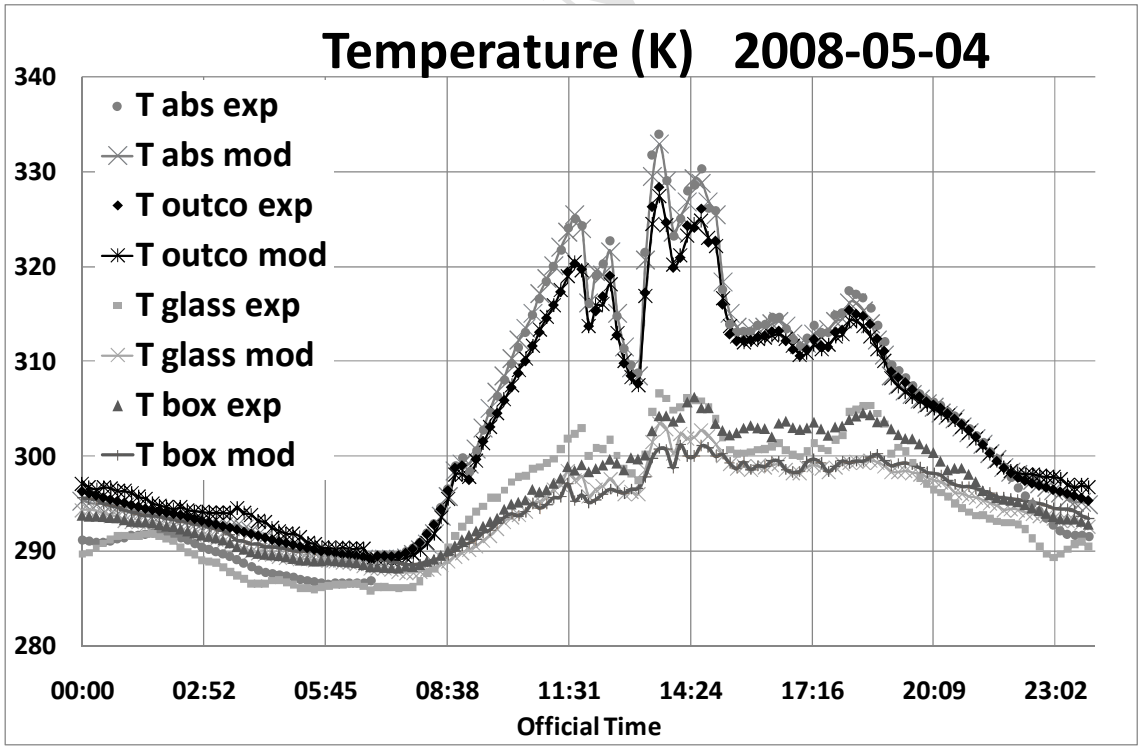

Figure 8: Collector model and experimental temperatures vs. the official summer time in Spain (UTC/GMT+2h) for 2008-09-14 (sunny day) and 2008-05-04 (cloudy day).

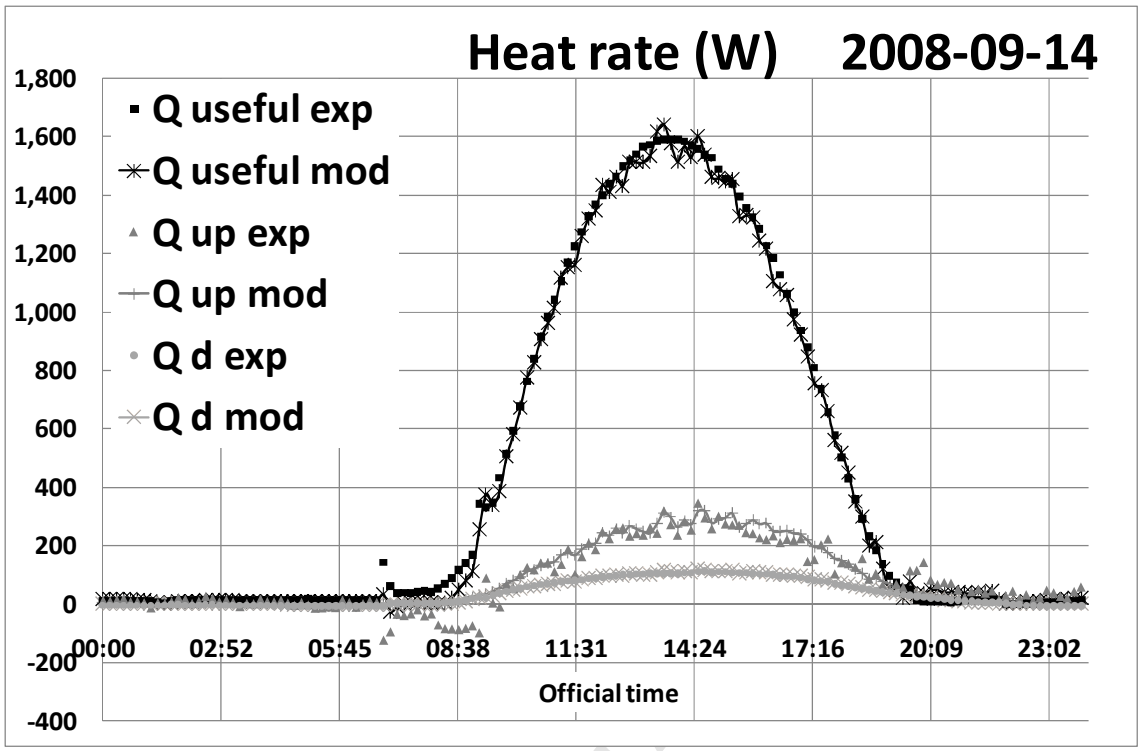

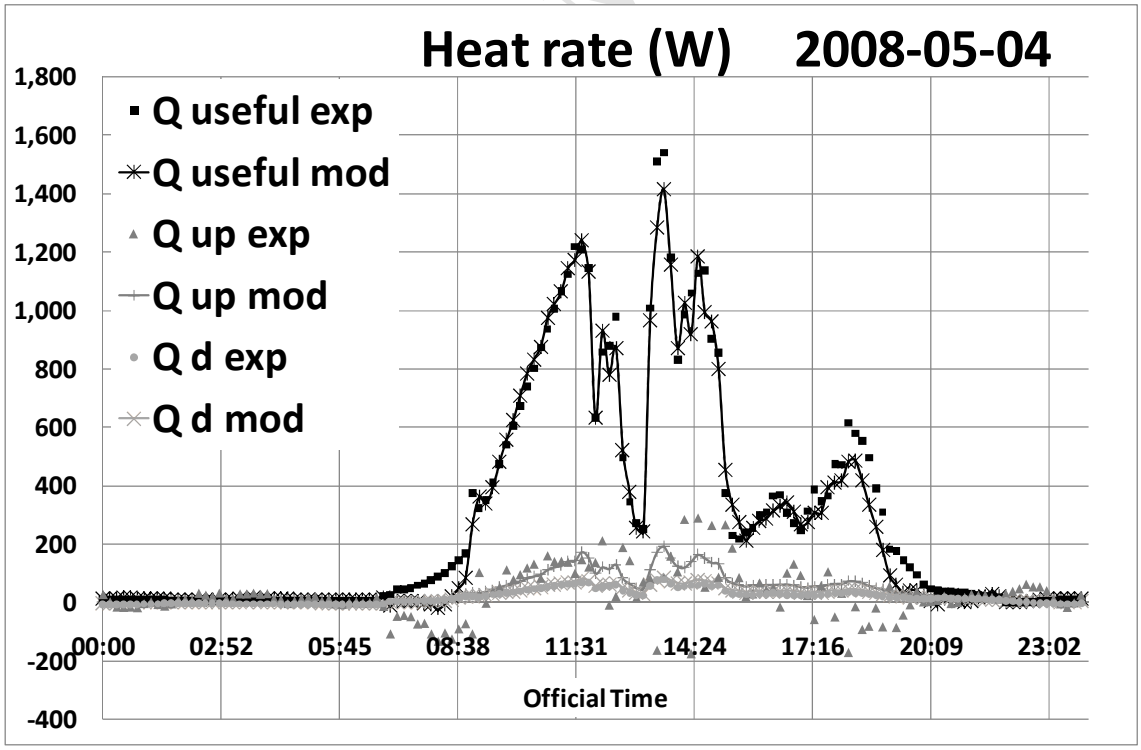

Figure 9: Collector heat rate distribution vs. official summer time. Model validation with experimental heat fluxes for 2008-09-14 (sunny day) and 2008-05-04 (cloudy day).

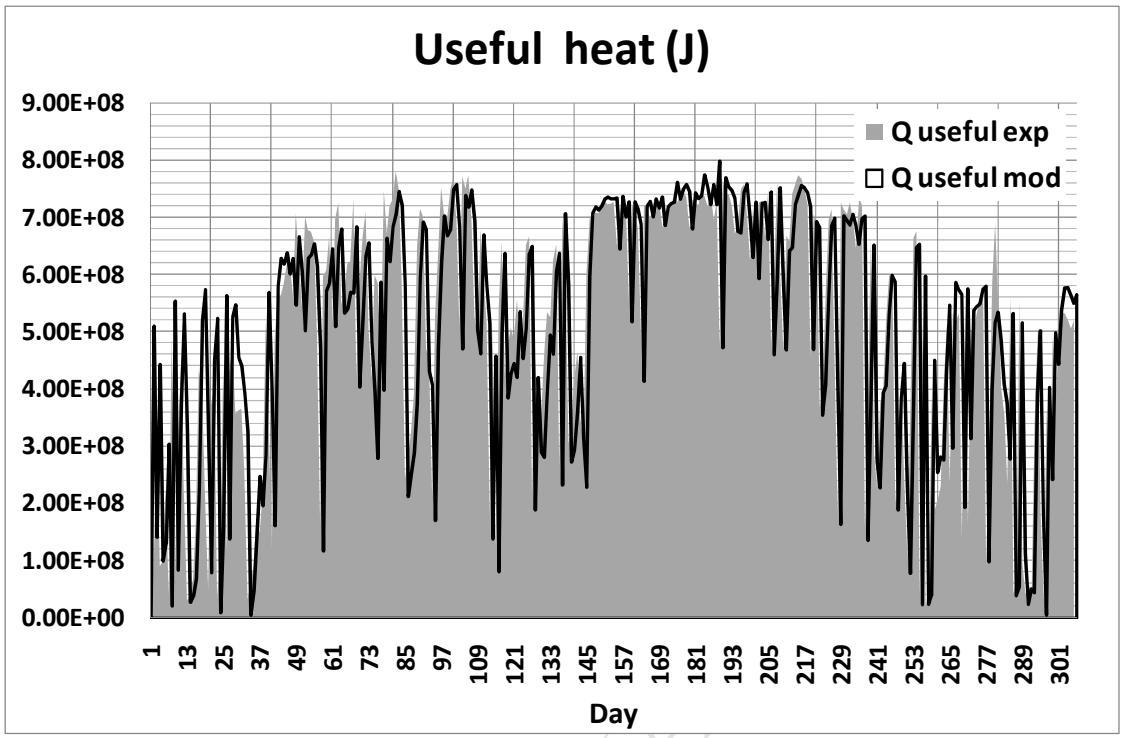

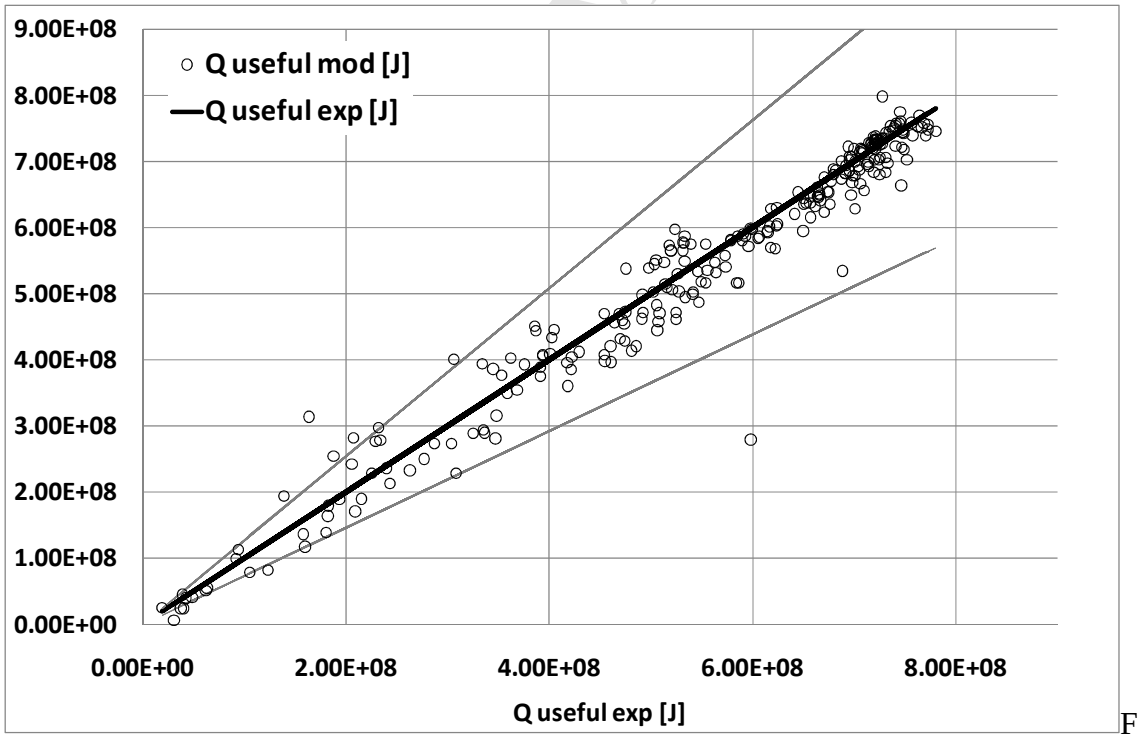

Figure 10: Comparison between the daily useful heat obtained from the model and the heat calculated through the experimental temperatures and mass flow rate over a year.

The auxiliary lines indicate the confidence interval as indicated in the text: 1.6% ± 27%.

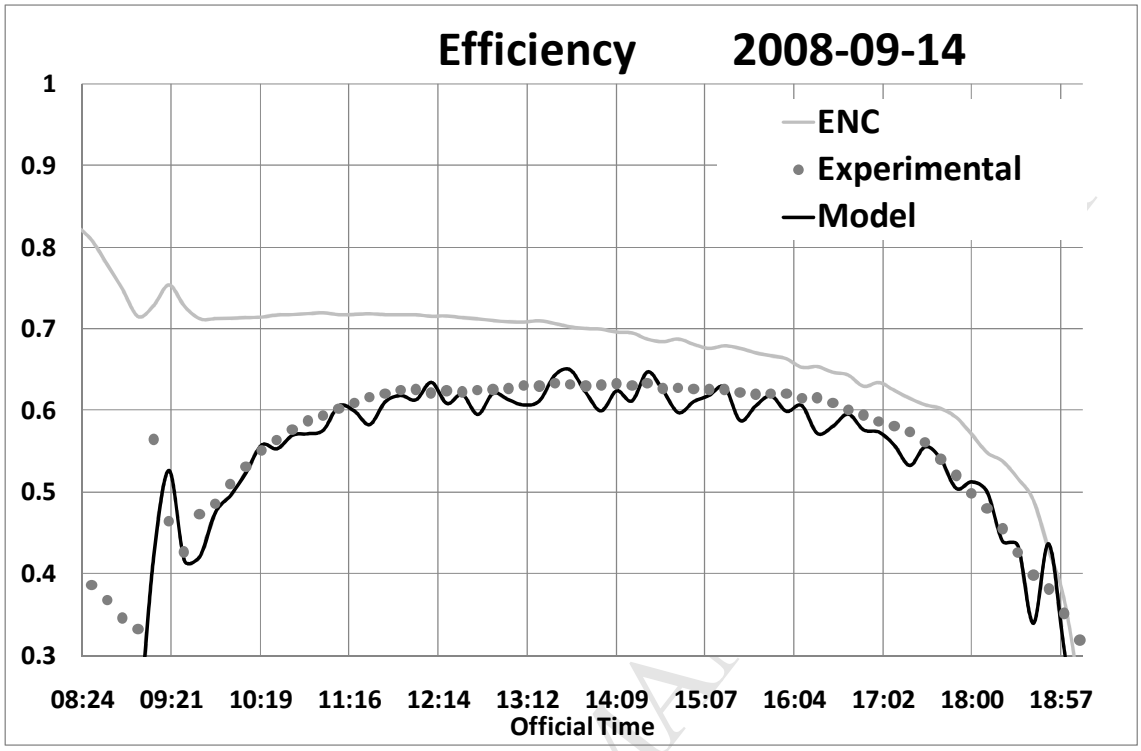
Efficiency 2008-09-14
ENC
Experimental
Model
1
0.9
0.8
0.7
0.6
0.5
0.4
0.3
08:24
09:21
10:19
11:16
12:14
13:12
14:09
15:07
16:04
17:02
18:00
18:57
Official Time

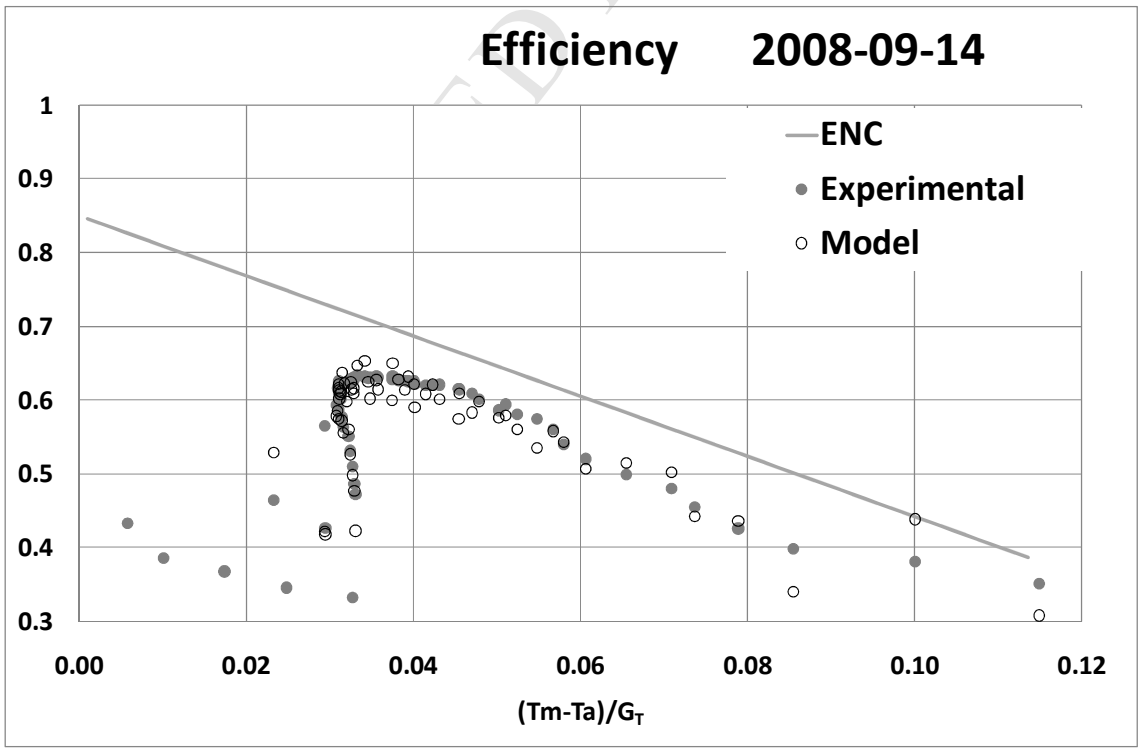
Efficiency 2008-09-14
ENC
Experimental
Model
1
0.9
0.8
0.7
0.6
0.5
0.4
0.3
0.00
0.02
0.04
0.06
0.08
0.10
0.12
(Tm-Ta)/G_T

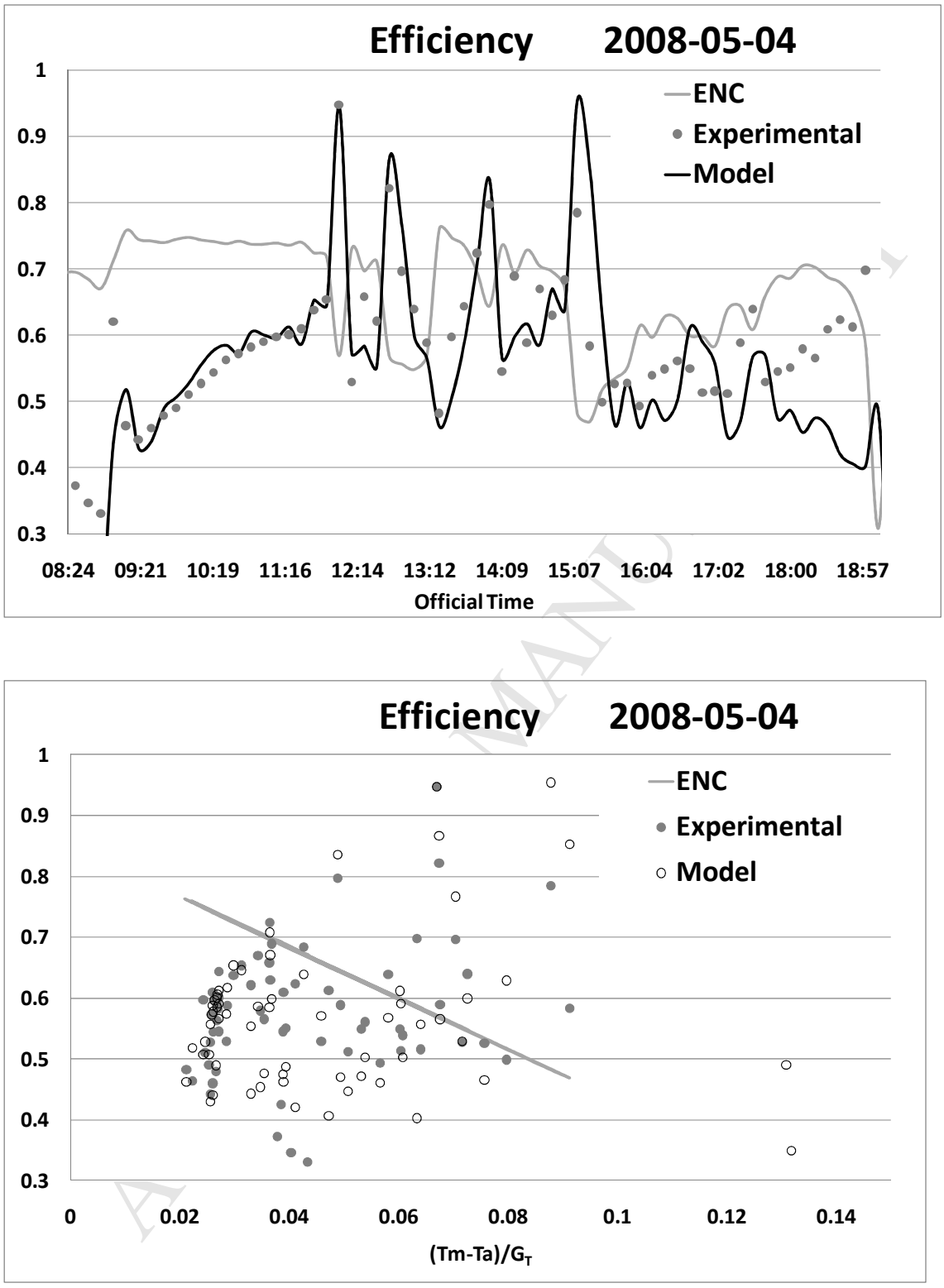

Figure 11: ENC, experimental and collector model efficiencies vs. the official summer time and the $\left(\frac{T_m - T_a}{G_T}\right)$ parameter for 2008-09-14 (sunny day) and 2008-05-04 (cloudy day).

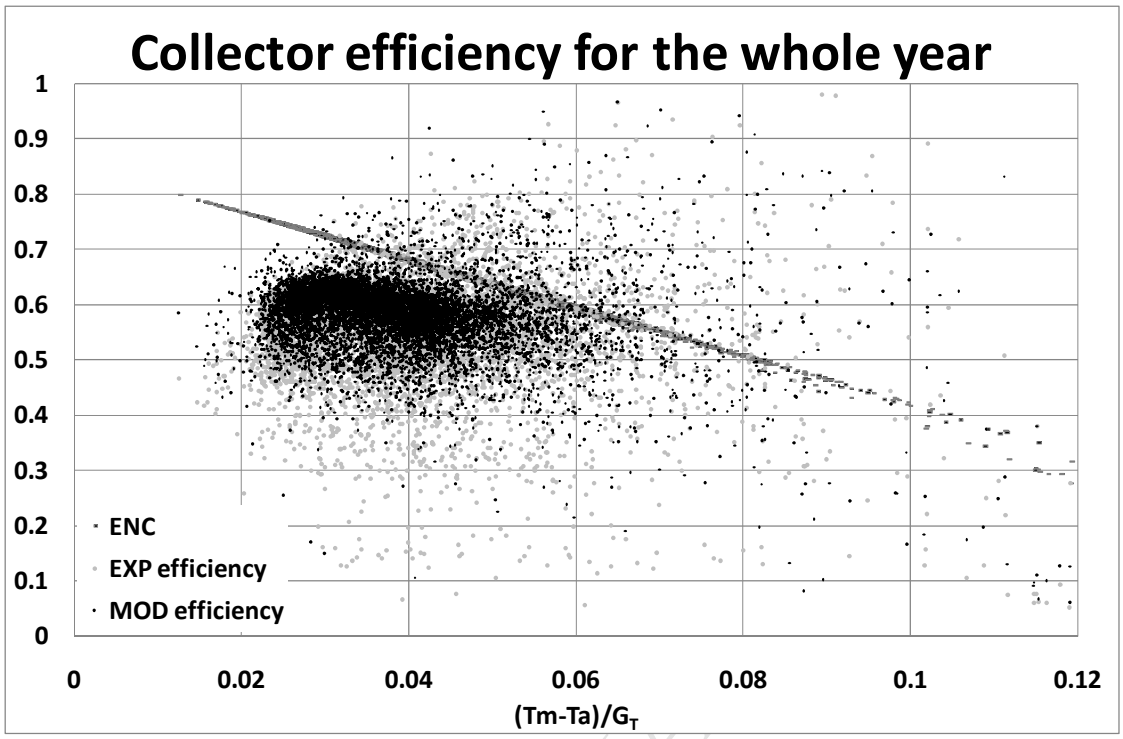

Figure 12: Collector efficiency. Experimental, collector model and normalization curve vs. $\left(\frac{T_m - T_a}{G_T}\right)$ parameter with a solar irradiance (G_T) threshold of 300 W m^{-2} over the entire year studied.